Published in final edited form as:

Int J Therm Sci. 2018 ; 126(Pt B): . doi:10.1016/j.ijheatmasstransfer.2018.06.077.

Specific heat of aluminum-oxide nanolubricants

Lingnan Lin[a,b,*] and **Mark A. Kedzierski**[a]

[a]National Institute of Standards and Technology, Gaithersburg, MD, USA

[b]Institute of Refrigeration and Cryogenics, Shanghai Jiao Tong University, Shanghai, China

Abstract

This paper presents specific heat measurements for a synthetic polyolester (POE) based aluminum oxide (Al_2O_3) nanolubricant with a polymeric surfactant over a temperature range from approximately 4 °C to 45 °C. Al_2O_3 nanolubricants with two nominal surface-area-based diameter nanoparticles were investigated: 20 nm and 40 nm. The number-based diameter of the nanoparticles, as determined by dynamic light scattering (DLS), were 112 nm and 148 nm, respectively. The nanoparticle mass fractions were varied from 0.076 to 0.249 for the 112-nm diameter nanolubricant, and from 0.059 to 0.394 for the 148-nm diameter nanolubricant. The measurements showed that the specific heat of the nanolubricant linearly increased with increasing temperature, and linearly decreased with respect to increasing nanoparticle mass fraction. The size of the nanoparticle was shown to have no effect on the magnitude of the specific heat of the nanolubricant. The measurements were compared with two existing models. The mass fraction weighted model exhibited excellent agreement with the measurements (within ±1.01%). In contrast, the volume mass fraction model failed to predict the measurements for most conditions to within ±5%.

Keywords

Air conditioning; Density; Lubricant; Nanofluid; Nanoparticles; Specific heat

1. Introduction

Heating, ventilation, air conditioning and refrigeration (HVAC&R) is a major energy consumption sector for most developed and some developing countries of the world. For this reason, researchers continue the quest for cost effective methods for improving the energy efficiency of HVAC&R equipment. The use of nanolubricants in chillers is a novel technique with the goal of increased efficiency. Compared with the neat lubricant, nanolubricants have beneficial properties that can improve heat transfer [1]. For example, Kedzierski [2] has shown that an aluminum-oxide (Al_2O_3) nanolubricant can improve the pool-boiling heat transfer of a refrigerant/lubricant by as much as 155%. Similarly, Bigi et al. [3] also reported

*Corresponding author at: National Institute of Standards and Technology, Gaithersburg, MD 20899, USA. lingnanlin@sjtu.edu.cn (L. Lin).

Conflicts of interest
None.

a 35% improvement of the refrigerant/lubricant convective boiling heat transfer coefficient by using Al_2O_3 nanolubricants in place of the base lubricant while having a small effect on pressure drop. In addition, nanolubricants have better tribological performance due to the ‘‘ball bearing” effect, thereby leading to a higher compressor efficiency [4,5]. Thus, nanolubricants have a significant potential for increasing the energy efficiency of HVAC&R equipment.

The specific heat (C_p) is a primary thermophysical property for thermal design. For example, the specific heat is essential for calculating single-phase heat transfer rates [6]. Moreover, nearly all turbulent single-phase convective flow and flow-boiling correlations include the Prandtl number ($Pr = \mu C_p/\lambda$), and some include the thermal diffusivity ($\alpha = \lambda/\rho C_p$) [7,8], which both require the C_p. The specific heat can also be used to calculate other properties such as the thermal expansion coefficient and the isothermal compressibility [9]. Therefore, nanolubricant specific heat measurements and corresponding models are required for the application of nanolubricants to HVAC&R equipment and other heat transfer applications.

Unfortunately, the available data for the specific heat of nanolubricants is limited. Only two studies were found in the literature that present measurements for the specific heat of nanolubricants. In the first study, Cremaschi et al. [10,11] measured the specific heat of two Al_2O_3/polyolester (POE) nanolubricants with nanoparticle mass fractions of 10% and 20% for five temperatures ranging from approximately 10 °C to 40 °C. They showed that the specific heat of the nanolubricant increased with temperature, but decreased with nanoparticle mass fraction. The Cremaschi et al. [10,11] study did not report the mass fraction of the surfactant, and was limited to a single base lubricant (RL32H[1]), with the Al_2O_3 nanoparticles consisting of a single gamma phase. In the second study, Lue et al. [12] measured the specific heat of a Al_2O_3 nanolubricant for vacuum pump applications for five nanoparticle mass fractions ranging from 0.1% to 1.6%. The specific heat of the Al_2O_3 nanolubricant was also shown to decrease with nanoparticle mass fraction. The Lue et al. [12] study limited to a specific vacuum-pump-oil base lubricant and it neglected to report the phase of the Al_2O_3 nanoparticles. Measurements of the specific heat for nanofluids other than nanolubricants are more numerous and have been made with base fluids like water [13–16], water/ethylene glycol [16–19], ethylene glycol [19,20], and molten salt [21,22]. As indicated by the above literature, the specific heat of a nanolubricant can be affected by temperature, nanoparticle mass fraction, and surfactant characteristics.

The objective of the present study is to expand on the specific heat database for Al_2O_3 nanolubricants by measuring the influence of temperature, nanoparticle size and mass fraction, and surfactant properties on the specific heat of several Al_2O_3 nanolubricants for a wide range of test conditions. This was done for a base lubricant and Al_2O_3 nanoparticles that differed from the ones used by Cremaschi et al. [10] and Lue et al. [12]. In addition, the present study reports the mass fraction of the surfactant in the nanolubricants, and the study aims to assess existing predictive methods for the specific heat of the Al_2O_3 nanolubricants.

[1]Certain commercial equipment, instruments, or materials are identified in this paper in order to specify the experimental procedure adequately. Such identification is not intended to imply recommendation or endorsement by the National Institute of Standards and Technology, nor is it intended to imply that the materials or equipment identified are necessarily the best available for the purpose.

2. Measurements

2.1. Test nanolubricants

The nanoparticles for the test nanolubricants were Al_2O_3 with crystal phase of 70% δ and 30% γ. The base lubricant for the nanolubricants was RL68H, a synthetic polyolester commercial chiller lubricant. A proprietary polymeric surfactant[2] was used to disperse the nanoparticles in the RL68H. Two different nanoparticle nominal, surface-area based diameters (D_{p0}) were used, 20 nm and 40 nm, as reported by the manufacturer. For each diameter, a concentrated nanolubricant made by a manufacturer was diluted by adding different masses of neat lubricant to provide five nanolubricants with varied nanoparticle mass fractions. The dilution process was performed by stirring the mixtures along with ultrasonication for approximately 24 h. The ratios of the mass of the surfactant to that of the nanoparticles (k) were approximately 0.3125 and 0.25 for the diameters 20 nm and 40 nm, respectively, and remained constant with the dilution process.

The size of the nanoparticles in the lubricant were measured with a dynamic light scattering (DLS) technique using a number-weighted basis. For spherical nanoparticles, the number-weighted DLS measurement more closely represents the average overall diameter than does the surface-area weighted basis because each nanoparticle diameter is equally weighted [23]. The DLS measurements were performed with a commercial instrument with a reported uncertainty of ±2%. All measurement uncertainties reported in this paper are for a 95% confidence level. The manufacturer's uncertainty was verified by using a NIST-traceable 60 nm ± 2.7 nm nanofluid standard. The measured diameter of the standard with the DLS instrument was 64 nm ± 5 nm, which coincides with the uncertainty range of the standard. Fig. 1 shows the number-weighted size distributions for the two undiluted nanolubricants. The number-weighted size gives each nanoparticle equal weight in determining the average, while the surface-area weighting more heavily weights nanoparticles with larger surface area. The surface-area weighted evaluation is more valuable than the number-weighted evaluation to a manufacturer of dispersions because it gives a better indication for the quantity of surfactant required to cover the surface of all the nanoparticles. The average diameters on number-weighted basis (D_p) were 112 nm and 148 nm, respectively. The width at half of the peak number percentage was roughly 29 nm for D_p = 112 nm (i.e., D_{p0} = 20 nm), and was 33 nm for D_p = 148 nm (i.e., D_{p0} = 40 nm). Potentially, a small portion of the difference between the DLS sizing and that of the manufacturer may be due to aggregation.[3] Nevertheless, similar differences between the present investigator's number-weighted measurements and the manufacturer's surface-area based technique have been experienced in previous investigations [23–25].

As reported by the manufacturer, the nanoparticle mass fractions for the undiluted nanolubricants were 0.249 and 0.394 for the diameters of 112 nm and 148 nm, respectively. For the diluted nanolubricants, the nanoparticle mass fractions were determined from the

[2]Due to the proprietary nature of the surfactant (Nanophase Technologies R&D product code R1103RL68H), no property information can be provided here.

[3]No particle settling was observed for the approximate month of testing, and the dispersion was believed to be stable based on this observation and the DLS measurements.

measured masses of the neat lubricant and the original nanolubricant that was combined to make the diluted nanolubri-cant. The mass fraction of the surfactant (x_s) was calculated by multiplying the nanoparticle mass fraction (x_{np}) with the ratio of the mass of surfactant to that of the nanoparticles (k). The k for the diameters of 112 nm and 148 nm were 0.3125 and 0.25, respectively, which remained constant with the dilution process. The mass fraction of the lubricant (x_L) was calculated by $x_L = 1 - x_s - x_{np}$. The mass fractions for the nanoparticles, the surfactant, and the lubricant are given in the column 3, 4, and 5 of Table 1, respectively.

The measured nanoparticle mass fractions were verified by using the measured densities of the nanolubricants. Kedzierski [23–25] has shown that the density of a nanolubricant with surfactant observes the suspension mixture equation:

$$\frac{1}{\rho_m} = \frac{x_{np}}{\rho_{np}} + \frac{x_s}{\rho_s} + \frac{x_L}{\rho_L} \quad (1)$$

where ρ_m, ρ_{np}, ρ_s, and ρ_L are the densities of the nanolubricants, the nanoparticles, the surfactant, and the lubricant, respectively. It's noted that Eq. (1) is equivalent to the density mixing law for mixture (i.e., the density of a mixture equals to the volume fraction weighted average of the density of each component). Substituting $x_s = kx_{np}$ and $x_L = 1 - x_s - x_{np}$ into Eq. (1) and rearranging for the nanoparticle mass fraction yields:

$$x_{np} = \left(\frac{1}{\rho_m} - \frac{1}{\rho_L}\right) / \left(\frac{1}{\rho_{np}} + \frac{k}{\rho_s} - \frac{k+1}{\rho_L}\right) \quad (2)$$

For verification purposes, the nanoparticle mass fractions were calculated with Eq. (2) using the measured densities of the nanolubricants and the known densities of the Al_2O_3 nanoparticles (3600 kg m^3, reported by Sarkas [26]), the surfactant (938.0 kg m^3, measured by Kedzierski [25]), and the lubricant (979.3 kg m^3, measured in the present study). All density measurements were performed on a Stabinger-type viscometer at a temperature of (20.00 ± 0.02) °C and at atmospheric pressure at an approximate altitude of 137 m above sea level (Gaithersburg, Maryland, USA). Complete details for the density measurement can be found in [23–25].

Table 2 compares the nanoparticle mass fractions that were determined by the measured masses to those determined by using the density measurements and Eq. (2). As can be seen, the deviation between the two methods remained within ±0.002, which provides a confirmation for the measurements of the mass fractions of the nanoparticles, and thereby, that for the surfactant and the lubricant.

2.2. Specific heat measurement

The specific heat was measured with a differential scanning calorimeter for a temperature range from 4 °C to 45 °C, which covered the temperatures applicable to water chillers.

As shown in Fig. 2, the primary working component of the calorimeter was a highly-thermally-conductive calorimetric block with two wells for holding a cell to contain the sample to be tested and an empty cell for reference. The metal calorimetric block was surrounded by Peltier-effect sensors to measure the heat flow through each cell and the temperature of the blocks, which is assumed to be the temperature of the sample. The high thermal conductivities of the sensors and the calorimetric block and the good thermal contact between them helped to promote a uniform temperature for the calorimetric block and its cells. The calorimetric block was housed within the innermost of three concentric chambers. Peltier elements within the intermediate and the outer chambers provided fine temperature control of the block in the inner chamber. The external chamber was cooled by a water circuit with a flow of approximately 12 L min^{1} and a thermostatically fixed temperature of (23.5 ± 0.2) °C. A constant flow of nitrogen gas was supplied to avoid condensation of water vapor on the walls of the calorimetric block at low temperature.

The ‘‘continuous method” was used to determine the specific heat for a temperature range. The block and cells were initially cooled to the lower-bound temperature and stabilized. Then the block and cells were heated at a constant rate to the upper-bound temperature, which was followed by another stabilization period. During this process, the calorimeter was used to measure the temporal heat flow (q) and the temperature (T) of the cell. The above procedures were repeated for the following two conditions: (1) the one test cell containing the sample with the other one being empty; and (2) both cells empty. Three data sets were obtained, i.e., q_1 vs t, q_2 vs t, and T vs t, where q_1 and q_2 are the heat flows through the test cell for conditions 1 and 2, respectively. The specific heat is defined as:

$$mC_p\frac{\mathrm{d}T}{\mathrm{d}t} = q \quad (3)$$

where m is the sample mass measured with a balance to within ±0.002 g with 95% confidence. By rearranging Eq. (3), the C_p can be calculated as a function of time and temperature:

$$C_p = (q_1 - q_2)/\left(m\frac{\mathrm{d}T}{\mathrm{d}t}\right) \quad (4)$$

where $(q_1 - q_2)$ is the net heat flow through the liquid sample.

In the present study, the stabilization periods before and after the heating period were both set to 40 min, and the rate of temperature increase for the heating period was set to 0.2 °C min^{-1}. These parameters were chosen because they produced the best agreement between the measurements for distilled water and a standard reference database for water as described in the next section. Because the specific heat measurement was obtained from fits of functional forms, which exhibit the largest uncertainties at the two ends of the range of the fit, measurements from these larger uncertainty regions were omitted. Consequently, the temperature range of the heating period was larger (1–48 °C) than the desired range so that only the smaller uncertainty data could be retained. The retained range of data for the

specific heat was for temperatures between approximately 4–45 °C with an interval of 0.5 °C.

For each measurement, the test cell was filled with approximately 0.8 mL of the liquid sample (about 80% of the cell volume), and then sealed with a threaded stopper and an O-ring. The sample mass was measured with an electronic balance having a resolution of 1 mg. The specific heat of the sample was then measured with the calorimeter following the aforementioned procedures. After that, the cell was readied for the next measurement by ultrasonic cleaning with alcohol and then drying by continuous evacuation. Three parallel measurements were performed for each nanolubri-cant concentration, which produced a total of 246 specific heat measurements.

2.3. Uncertainties

All uncertainties given in this paper are for the 95% confidence level unless otherwise stated. The uncertainty of the nanoparticle mass fractions (x_{np}), the surfactant mass fractions (x_s), and the lubricant mass fractions (x_L) were approximately ±0.02%.[4] The uncertainty of nanolubricant density was within ±0.26%.

In order to evaluate the uncertainty of the specific heat measurement, the specific heat of a distilled water sample was measured and compared to the reference value from the NIST Reference Fluid Thermodynamic and Transport Properties Database (REFPROP) [27]. As shown by Fig. 3, the shape of the measurement curve is approximately the same as that of the reference, and there is approximately a 0.02 kJ kg^{-1} K^{-1} fixed offset between the mean of the measurements and the reference. The root-mean-square of the difference between the measurement and the reference was 0.6% of the measurement. The system uncertainty for the specific heat measurement was estimated by multiplying the0.6% by a coverage factor and combining it with the uncertainty for the reference standard (0.1% [27]), resulting in 1.18%. The expanded uncertainty of the specific heat ($U_{r,Cp}$) for each fluid was calculated by combining the system uncertainty with the standard uncertainties of the regressions with a coverage factor. The standard uncertainty of a regression was evaluated by the residual standard deviation of fit. The last column of Table 1 gives the calculated specific heat uncertainties for each test fluid. It was shown that the specific heat uncertainties for all the test nanolubricants and the neat lubricant were within 1.21%, while that for the lubricant/surfactant mixture (50/50 by mass) was 1.75%.

3. Results and discussion

3.1. Specific heat of lubricant, surfactant, and nanoparticles

The measured specific heat of the neat lubricant (RL68H) and the lubricant/surfactant mixture (50/50 by mass[5]) are shown in Fig. 4. A total of 246 data points were included for each of the test fluids. The specific heats for the neat lubricant and for the lubricant/surfactant mixture are approximately linear with respect to the temperature. The best linear fits (or estimated means) are shown by solid lines in Fig. 4, and the fitting constants are

[4]The uncertainties with unit of % refer to relative uncertainties, i.e., the percentage of absolute uncertainty to measurement.
[5]The 50/50 lubricant/surfactant mixture was prepared and supplied by the manufacturer.

given in Table 1. The shaded areas to either side of the fitting lines represent the 95% confidence intervals. As the temperature increases from 4 °C to 45 °C, the estimated mean specific heat of the neat lubricant increases from 1.81 kJ kg^{-1} K^{-1} to 1.91 kJ kg^{-1} K^{-1}, and that of the lubricant/surfactant mixture increases from 1.95 kJ kg^{-1} K^{-1} to 2.03 kJ kg^{-1} K^{-1}. The larger variation from the straight-line exhibit by the 50/50 lubricant/surfactant mixture as compared to the neat lubricant is hypothesized as being due to some surfactant aggregation. In general, surfactants have a greater propensity for aggregation at high concentration [28]. Aggregation provides the potential for density gradients and buoyancy mixing that could affect the stability of the measurements.

The specific heat of the neat surfactant ($C_{p,s}$) was calculated from the estimated mean specific heat of the neat lubricant ($C_{p,L}$) and the 50/50 lubricant/surfactant mixture ($C_{p,Ls}$) using the recommended equation for liquid mixtures [29]:

$$C_{p,\mathrm{Ls}} = x_{\mathrm{L}} C_{p,\mathrm{L}} + x_{\mathrm{s}} C_{p,\mathrm{s}} \quad (5)$$

where x_{L} and x_{s} are both equal to 0.5. The constants for the derived linear fit for the $C_{p,s}$ are shown in the third row of Table 1. The residual standard deviation for the fit of $C_{p,s}$ was obtained by combining that of $C_{p,Ls}$ and $C_{p,L}$ with a coverage factor. The expanded uncertainty of the specific heat of surfactant was calculated to be 1.76%. Fig. 4 shows the calculated specific heat of the surfactant versus the temperature with a solid line and shaded areas to either side representing the 95% confidence interval.

Because the Al_2O_3 nanoparticles used in this study have two crystal phases, δ and γ, with mass fractions of 70% and 30%, respectively, the specific heat of the δ/γ-phase Al_2O_3 nanoparticle was estimated by the mass-weighted average of each crystal phase. The single-crystal-phase Al_2O_3 nanoparticle was calculated as [30]:

$$C_p[\mathrm{Jkg^{-1}K^{-1}}] = \frac{B_1 + B_2\frac{T[\mathrm{K}]}{1000} + B_3\left(\frac{T[\mathrm{K}]}{1000}\right)^2 + B_4\left(\frac{T[\mathrm{K}]}{1000}\right)^3 + B_5\left(\frac{T[\mathrm{K}]}{1000}\right)^{-2}}{M[\mathrm{kgmol^{-1}}]} \quad (6)$$

where the constants B_1–B_5, which were taken from Domalski and Hearing [30], are given in Table 3; and M is the molar mass of Al_2O_3, which is equal to 0.1016913 kg mol^{-1}. Fig. 5 shows the calculated specific heat of the δ-phase, γ-phase, and δ/γ-phase Al_2O_3. The specific heat of the δ/γ-phase Al_2O_3 was calculated by linearly weighting the δ-phase and the γ-phase values by mass fraction. As the temperature increases from 4 °C to 45 °C, the specific heat of the δ/γ-phase Al_2O_3 increases from 0.74 kJ kg^{-1} K^{-1} to 0.85 kJ kg^{-1} K^{-1}, which is, on average, 43% of the specific heat of the neat lubricant.

3.2. Nanolubricant specific heat measurements

Figs. 6 and 7 show the measured specific heat of the nanolubricants for the diameters of 112 nm and 148 nm, respectively. A total of 246 data points were included for each of the test nanolubricants. As can be seen, the specific heat of the nanolubricant increases linearly with

respect to temperature. The solid lines shown in Figs. 6 and 7 are linear best-fit regressions (or estimated means) of the data. The shaded areas to either side of the fitting lines represent the 95% confidence intervals, though they are diffi-cult to see on the figures because they nearly coincide with the mean values. Table 1 gives the constants for the linear regressions of the measured specific heat versus the temperature for the tested nanolubricants, along with the residual standard deviation of each fit.

Fig. 8 plots the specific heat versus the nanoparticle mass fraction for temperatures of 5 °C and 44 °C and for nanoparticle diameters of 112 nm and 148 nm. In Fig. 8, the plotted data for specific heat was calculated from the linear best-fit regressions shown in Table 1 for a given temperature. The vertical bars represent the expanded uncertainty for 95% confidence interval for the specific heat, which were calculated from the $U_{r,Cp}$ values that are given in Table 1. The lines (dashed or solid) were the linear best-fit regressions for the data points. As shown in Fig. 8, the specific heat exhibits a linear decreasing trend with the nanoparticle mass fraction, and the decreasing rate with respect to nanoparticle mass fraction are nearly the same for different temperatures or for different nanoparticle diameters. On the other hand, the specific heat for 112 nm is slightly lower than that for 148 nm (on average, 0.4% lower for 5 °C, and 0.5% lower for 44 °C). However, the difference between the two is within the measurement uncertainty (1.21% in maximum); thus, it cannot be concluded that the nanoparticle size has an obvious effect on the specific heat of the nanolubricant.

3.3. Nanolubricant specific heat predictions

Two types of models have been used to predict the specific heat of a nanofluid: the volume fraction weighted model [31] and the mass fraction weighted model [32]. The volume fraction weighted model assumes that the specific heat is equal to the volume fraction weighted average of the specific heats of the base fluid and the nanoparticles, which is analogous to the mixing theory for ideal gas mixtures. The mass fraction weighted model is based on thermal equilibrium. Here, the specific heat is equal to the mass fraction weighted average of the specific heats of the base fluid and the nanoparticles. The two models produce nearly the same results for small nanoparticle concentration, but diverge greatly as the nanoparticle concentration increases. Researchers have shown that the mass fraction weighted model exhibits better agreement for nanofluid specific heat data [13,15,16,19]. A few empirical correlations were also proposed for the specific heat of a particular nanofluid [7,16,19,33].

Recently, the ‘‘nanolayer effect” has been considered in some models for the specific heat of molten-salt nanofluids [34]. The nanolayer effect refers to the phenomenon where the liquid molecules form an ordered, thin (a few nanometers), solid-like layer on the nanoparticle surface, which is thought to affect the heat exchange between the liquid and the nanoparticle. Although a few studies have shown that the nanolayer effect plays an important role for determining the thermal conductivity of nanofluids [35], its significance for the specific heat is not well understood. Nevertheless, some studies have shown that the nanolayer effect for the specific heat is particle size-dependent, i.e., the effect is more significant for smaller nanoparticles [36]. Being that our measurements have shown that the particle size does not have an obvious effect on the specific heat (Fig. 8), it is reasonable to

speculate that the nanolayer effect for the specific heat, of at least the present nanolubricants, can be neglected.

The volume fraction weighted model for the specific heat of the nanolubricant can be expressed as

$$C_{p,\mathrm{m}} = \phi_{\mathrm{np}} C_{p,\mathrm{np}} + \phi_{\mathrm{s}} C_{p,\mathrm{s}} + \phi_{\mathrm{L}} C_{p,\mathrm{L}} \quad (7)$$

where ϕ_{np}, ϕ_{s}, and ϕ_{L} are the volume fractions of nanoparticles, surfactant, and lubricant, respectively. The specific heats of the nanolubricants were calculated by Eq. (7) to compare with the measurements. The volume fractions used in Eq. (7) were calculated by $\phi_i = x_i \rho_m / \rho_i$, using the mass fractions and nanolubricant densities given in Table 1, and the densities of the Al_2O_3 nanoparticles (3600 kg m^3, reported by Sarkas [26]), the surfactant (938.0 kg m^{-3}, measured by Kedzierski [25]), and the lubricant (979.3 kg m^3, measured by Kedzierski [25]). The neat specific heats of the nanoparticles, the surfactant, and the lubricant have been given in Section 3.1. Fig. 9 plots the specific heat predicted by Eq. (7) versus the corresponding measurement for all data sets. As can be seen, Eq. (7) failed to predict the specific heat of the nanolubricants for most cases, though it predicted the measurements to within ±5% for the low nanoparticle mass fractions. The deviation between the prediction by Eq. (7) and the corresponding measurement increased dramatically with increasing nanoparticle mass fraction. For the nanoparticle (148 nm diameter) mass fraction of 0.394, the deviation reached approximately ±20%.

The mass fraction weighted model for the specific heat of the nanolubricant can be expressed as

$$C_{p,\mathrm{m}} = x_{\mathrm{np}} C_{p,\mathrm{np}} + x_{\mathrm{s}} C_{p,\mathrm{s}} + x_{\mathrm{L}} C_{p,\mathrm{L}} \quad (8)$$

For model verification, the specific heats of the nanolubricants were calculated by Eq. (8) using the specific heats of the nanoparticles, the surfactant, and the lubricant as given in Section 3.1 and the mass fractions given in Table 1. Fig. 10 plots the specific heat predicted by Eq. (8) versus the corresponding measurement for all data sets. As shown in Fig. 10, the prediction by Eq. (8) was in good agreement with the measurements for all data sets. No obvious dependency of the deviation with the nanoparticle mass fraction or size was observed. The maximal deviation was ±1.01%, which was less than the measurement uncertainty (±1.21% in maximum). The average deviation was ±0.37%. Thus, it is reasonable to state that the mass fraction weighted model (Eq. (8)) is sufficient to describe the specific heat of the nanolubricant. Given that Eq. (8) is based on macro properties of the components, and that the nanoparticle size was shown to not be an influential factor, it is believed that it could be used to predict the specific heat for nanolubricants of all base lubricants and all spherical nanoparticle materials of various diameters.

4. Conclusions

The specific heat of a synthetic polyolester-based Al_2O_3 nanolubricant with a polymeric surfactant for chiller application was measured for a temperature range from approximately 4 °C to 45 °C. Two nanoparticle diameters were investigated: 112 nm and 148 nm, which were determined by a DLS measurement on a number-weighted basis. The nanoparticle mass fractions of the test nanolubricants varied from 0.076 to 0.249 for a diameter of 112 nm and from 0.059 to 0.394 for the 148 nm diameter. The measurements were compared with two existing models. The following conclusions were obtained.

(1) The specific heat of the Al_2O_3 nanolubricant linearly increased with increasing temperature, and linearly decreased with increasing nanoparticle mass fraction.

(2) The nanoparticle size has no influence on the specific heat of the nanolubricant within the uncertainties of the measurements.(3) The mass fraction weighted model was sufficient to describe the specific heat of the nanolubricants. The model predicted the measured specific heats to within ±1.01%, which was less than the measurement uncertainty (±1.21% in maximum). The mass fraction weighted model is believed to be valid for all nanolubricants with spherical nanoparticles. On the other hand, the volume fraction weighted model failed to predict the measurements for most conditions to within ±5%.

Acknowledgements

This work was funded by NIST. The authors thank the following for their constructive criticism of the first draft of the manuscript: P. Domanski, and A. Pertzborn from NIST, and L. Cremaschi from Auburn University. The author Lingnan Lin thanks the China Scholarship Council (CSC) for his scholarship.

Nomenclature

English symbols

$\mathbf{A_n}$	constants in Table 1, $n = 1, 2$
$\mathbf{B_n}$	constants in Eq. (6), $n = 1, 2, 3, 4, 5$
$\mathbf{C_p}$	specific heat [kJ kg^{-1} K^{-1}
$\boldsymbol{D_p}$	nominal diameter of nanoparticles [nm]
$\boldsymbol{D_{p0}}$	primary diameter of nanoparticles [nm]
k	ratio of the mass of surfactant to that of nanoparticles
M	molecular mass [kg mol^{-1}]
m	mass [kg]
Pr	Prandtl number
q	heat flow [W]
T	temperature [°C or K]

t	time [s]
$\boldsymbol{U_{r,Cp}}$	expanded uncertainty of specific heat [%]
$\boldsymbol{U_{r,xn}}$	expanded uncertainty of nanoparticle mass fraction [%]
x	mass fraction

Greek symbols

α	thermal diffusivity [$m^2\ s^{-1}$]
γ	Al_2O_3 nanoparticle crystal phase [–]
δ	Al_2O_3 nanoparticle crystal phase [–]
ρ	density [$kg\ m^{-3}$]
ϕ	volume fraction
μ	dynamic viscosity [Pa s]
λ	thermal conductivity [$W\ m^{-1}\ K^{-1}$]

Subscripts

L	lubricant
Ls	lubricant/surfactant mixture
m	mixture
np	nanoparticles
s	surfactant

Abbreviation

DLS	dynamic light scattering
HVAC&R	heating, ventilation, air conditioning and refrigeration
NIST	National Institute of Standards and Technology
POE	polyolester

References

[1]. Azmi WH, Sharif MZ, Yusof TM, Mamat R, Redhwan AAM, Potential of nanorefrigerant and nanolubricant on energy saving in refrigeration system – a review, Renew. Sustain. Energy Rev 69 (2017) 415–428, 10.1016/j.rser.2016.11.207.

[2]. Kedzierski MA, Effect of Al2O3 nanolubricant on R134a pool boiling heat transfer, Int. J. Refrig 34 (2011) 498–508,

[3]. Bigi AAM, Cremaschi L, Deokar P, Nanolubricants flow boiling heat transfer enhancement in a microfin tube evaporator—IRG0021, Sci. Technol. Built Environ 23 (2017) 960–969, 10.1080/23744731.2017.1333347.

[4]. Tao X, Jiazheng Z, Kang X, The ball-bearing effect of diamond nanoparticles as an oil additive, J. Phys. D. Appl. Phys 29 (1996) 2932–2937, 10.1088/0022-3727/29/11/029.

[5]. Bi SS, Shi L, Zhang LL, Application of nanoparticles in domestic refrigerators, Appl. Therm. Eng 28 (2008) 1834–1843, 10.1016/j.applthermaleng.2007.11.018.

[6]. Webb RL, Kim N-H, Principles of Enhanced Heat Transfer, second ed, Taylor & Francis, New York, 2005.

[7]. Vajjha RS, Das DK, A review and analysis on influence of temperature and concentration of nanofluids on thermophysical properties, heat transfer and pumping power, Int. J. Heat Mass Transf 55 (2012) 4063–4078, 10.1016/j.ijheatmasstransfer.2012.03.048.

[8]. Vajjha RS, Das DK, Kulkarni DP, Development of new correlations for convective heat transfer and friction factor in turbulent regime for nanofluids, Int. J. Heat Mass Transf 53 (2010) 4607–4618,

[9]. Gaskell DR, Introduction to the Thermodynamics of Materials, fifth ed., CRC Press, Boca Raton, FL, USA, 2008.

[10]. Cremaschi L, Wong T, Bigi AAM, Thermodynamic and Heat Transfer Properties of Al2O3 Nanolubricants, in: 15th Int. Refrig. Air Cond. Conf., Purdue, IN, USA, 2014 p. Paper 1500.

[11]. Cremaschi L, Bigi AAM, Wong T, Deokar P, Thermodynamic properties of Al2O3 nanolubricants: Part 1—Effects on the two-phase pressure drop, Sci. Technol. Built Environ 21 (2015) 607–620, 10.1080/23744731.2015.1023165.

[12]. Lue YF, Hsu YC, Teng TP, Performance evaluation on vacuum pumps using nanolubricants, J. Mech. Sci. Technol 30 (2016) 4275–4283, 10.1007/s12206-016-0840-z.

[13]. O'Hanley H, Buongiorno J, McKrell T, Hu L, Measurement and model validation of nanofluid specific heat capacity with differential scanning calorimetry, Adv. Mech. Eng 4 (2012) 181079, 10.1155/2012/181079.

[14]. Parametthanuwat T, Bhuwakietkumjohn N, Rittidech S, Ding Y, Experimental investigation on thermal properties of silver nanofluids, Int. J. Heat Fluid Flow 56 (2015) 80–90, 10.1016/j.ijheatfluidflow.2015.07.005.

[15]. Zhou S-Q, Ni R, Measurement of the specific heat capacity of water-based Al_2O_3 nanofluid, Appl. Phys. Lett 92 (2008) 93123, 10.1063/1.2890431.

[16]. Vajjha RS, Das DK, Specific heat measurement of three nanofluids and development of new correlations, J. Heat Transf 131 (2009) 71601, 10.1115/1.3090813.

[17]. Spernarth L, Magdassi S, Preparation of ethyl cellulose nanoparticles from nano-emulsion obtained by inversion at constant temperature, Micro Nano Lett 2 (2007) 90–95, 10.1049/mnl.

[18]. Selvam C, Mohan Lal D, Harish S, Thermal conductivity and specific heat capacity of water–ethylene glycol mixture-based nanofluids with graphene nanoplatelets, J. Therm. Anal. Calorim 129 (2017) 947–955, 10.1007/s10973-017-6276-6.

[19]. Cabaleiro D, Gracia-Fernández C, Legido JL, Lugo L, Specific heat of metal oxide nanofluids at high concentrations for heat transfer, Int. J. Heat Mass Transf 88 (2015) 872–879,

[20]. Zhou L-P, Wang B-X, Peng X-F, Du X-Z, Yang Y-P, On the Specific Heat Capacity of CuO Nanofluid, Adv. Mech. Eng 2 (2010) 172085, 10.1155/2010/172085.

[21]. Lu M-C, Huang C-H, Specific heat capacity of molten salt-based alumina nanofluid, Nanoscale Res. Lett 8 (2013) 292, 10.1186/1556-276X-8-292. [PubMed: 23800321]

[22]. Jo B, Banerjee D, Enhanced specific heat capacity of molten salt-based carbon nanotubes nanomaterials, J. Heat Transf 137 (2015) 91013, 10.1115/1.4030226.

[23]. Kedzierski MA, Brignoli R, Quine KT, Brown JS, Viscosity, density, and thermal conductivity of aluminum oxide and zinc oxide nanolubricants, Int. J. Refrig 74 (2017) 3–11, 10.1016/j.ijrefrig.2016.10.003. [PubMed: 28736463]

[24]. Kedzierski MA, Viscosity and density of CuO nanolubricant, Int. J. Refrig 35 (2012) 1997–2002, 10.1016/j.ijrefrig.2012.06.012.

[25]. Kedzierski MA, Viscosity and density of aluminum oxide nanolubricant, Int. J. Refrig 36 (2013) 1333–1340, 10.1016/j.ijrefrig.2013.02.017.

[26]. Sarkas H, Private Communications, Nanophase Technologies Corporation, Romeoville, IL, USA, 2009.

[27]. Lemmon EW, Huber ML, McLinden MO, NIST Standard Reference Database 23: Reference Fluid Thermodynamic and Transport Properties (REFPROP), Version 9.0, 2010.

[28]. Mittal KL, Shah DO, Adsorption and Aggregation of Surfactants in Solution, CRC Press, Boca Raton, FL, USA, 2002.

[29]. Teja AS, Simple method for the calculation of heat capacities of liquid mixtures, J. Chem. Eng. Data 28 (1983) 83–85, 10.1021/je00031a025.

[30]. Domalski ES, Hearing ED, Condensed Phase Heat Capacity Data, in: Linstrom PJ, Mallard WG (Eds.), NIST Chem. WebBook, NIST Stand. Ref. Database Number 69, National Institute of Standards and Technology, Gaithersburg MD, 20899, 2017.

[31]. Pak BC, Cho YI, Hydrodynamic and heat transfer study of dispersed fluids with submicron metallic oxide particles, Exp. Heat Transf 11 (1998) 151–170, 10.1080/08916159808946559.

[32]. Xuan Y, Roetzel W, Conceptions for heat transfer correlation of nanofluids, Int. J. Heat Mass Transf 43 (2000) 3701–3707, 10.1016/S0017-9310(99)00369-5.

[33]. Fakoor Pakdaman M, Akhavan-Behabadi MA, Razi P, An experimental investigation on thermo-physical properties and overall performance of MWCNT/heat transfer oil nanofluid flow inside vertical helically coiled tubes, Exp. Therm. Fluid Sci 40 (2012) 103–111, 10.1016/j.expthermflusci.2012.02.005.

[34]. Khanafer K, Tavakkoli F, Vafai K, AlAmiri A, A critical investigation of the anomalous behavior of molten salt-based nanofluids, Int. Commun. Heat Mass Transf 69 (2015) 51–58, 10.1016/j.icheatmasstransfer.2015.10.002.

[35]. Angayarkanni SA, Philip J, Review on thermal properties of nanofluids: recent developments, Adv. Colloid Interface Sci 225 (2015) 146–176, 10.1016/j.cis.2015.08.014. [PubMed: 26391519]

[36]. Hentschke R, On the specific heat capacity enhancement in nanofluids, Nanoscale Res. Lett 11 (2016) 88, 10.1186/s11671-015-1188-5. [PubMed: 26873263]

[37]. Instrumentation SETARAM, Brochure of micro DSC 7 evo, Caluire, France, 2016 http://www.setaram.com/wp-content/uploads/2016/11/mDSC7-EVO.pdf.

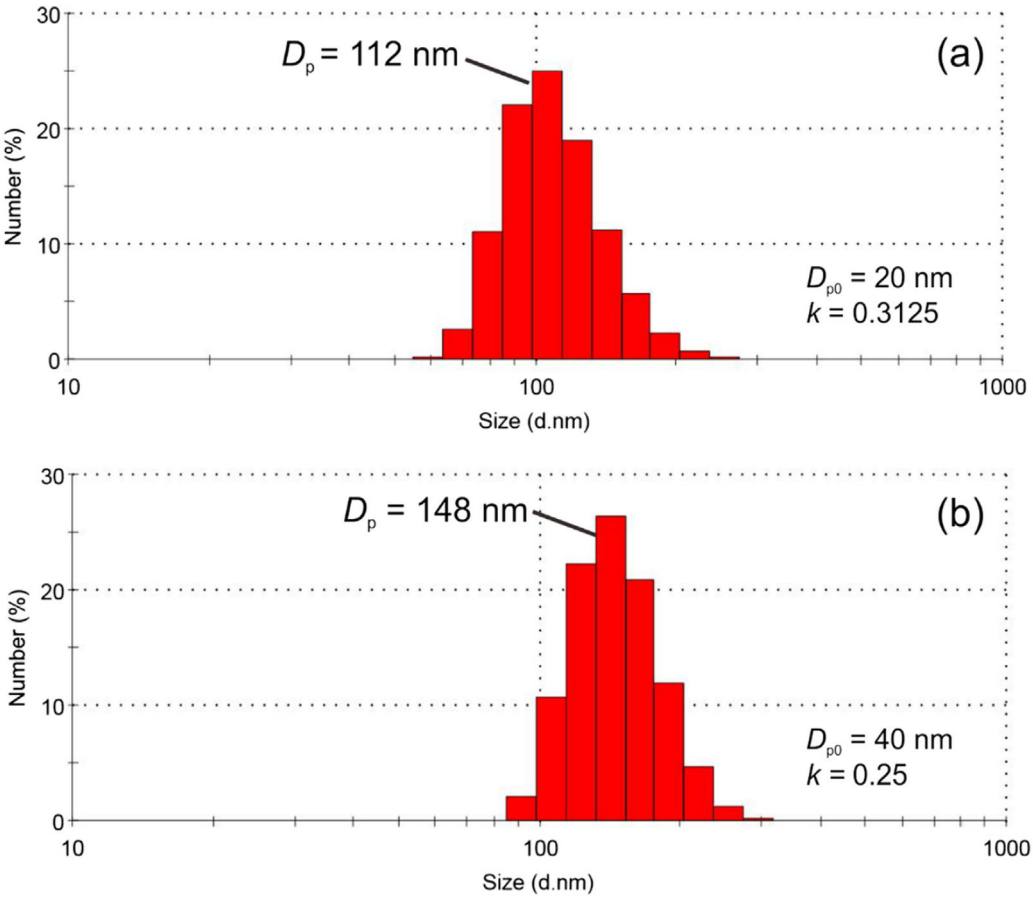

Fig. 1.

Representative size distributions by number-weighted basis for the 112-nm and the 148-nm diameter nanolubricants.

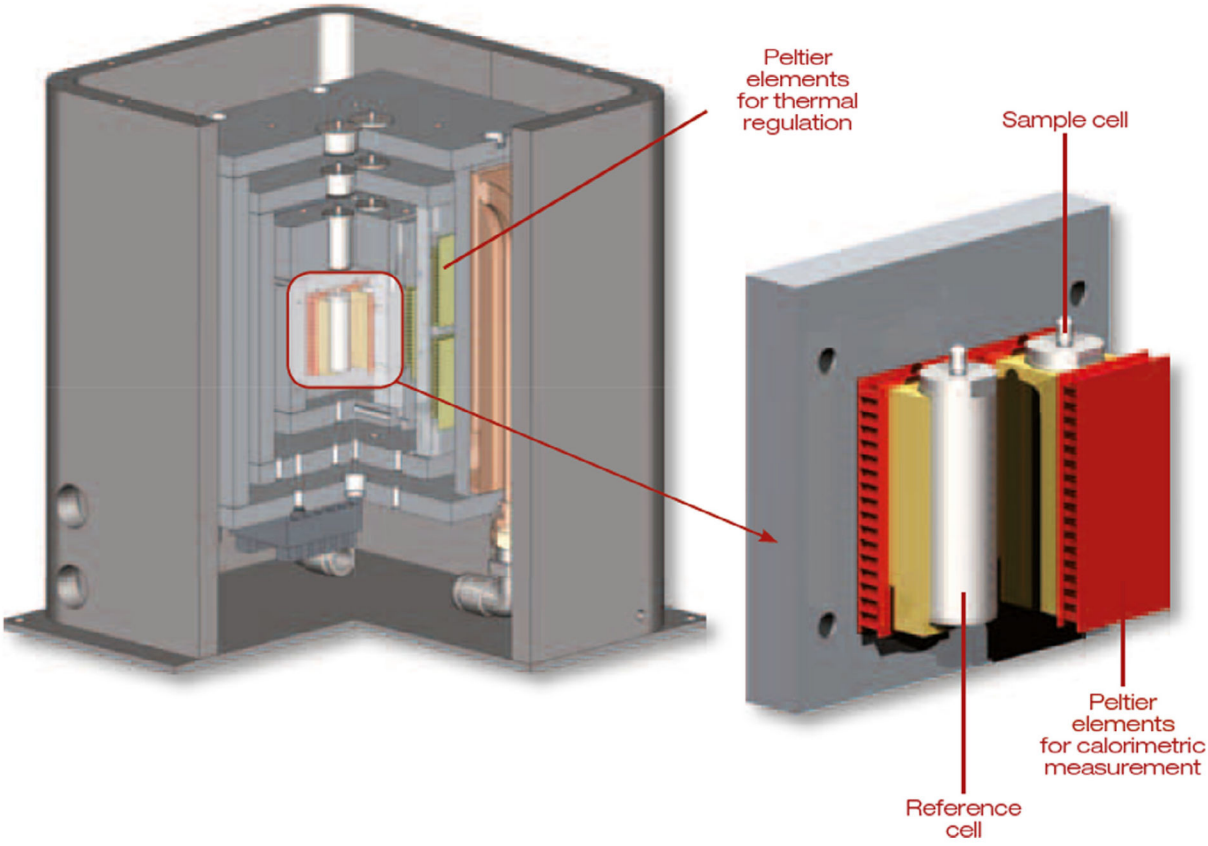

Fig. 2.
Schematic of the calorimeter [37].

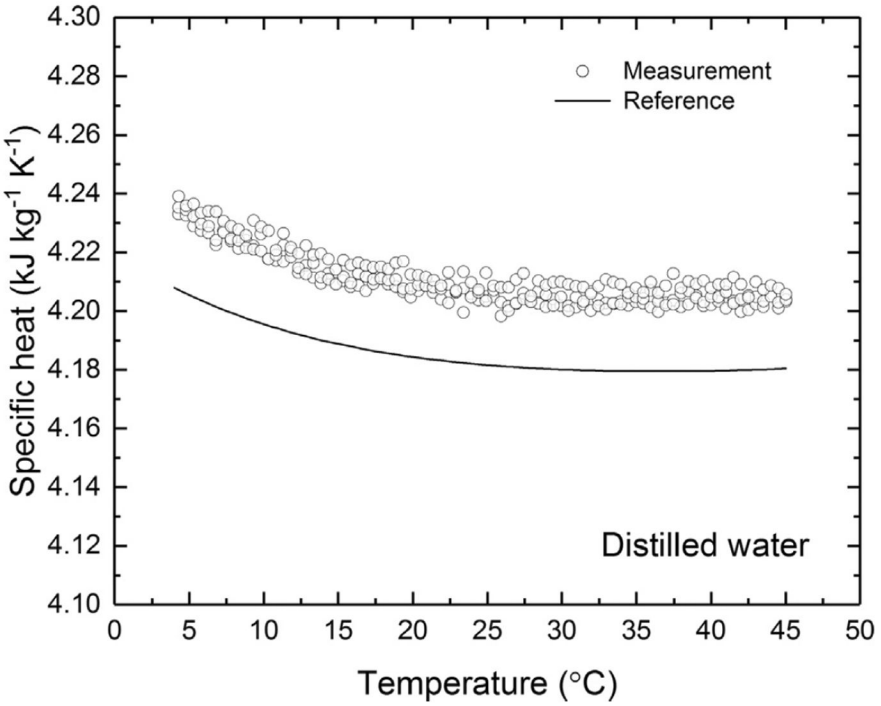

Fig. 3.
Measurement and reference for the specific heat of distilled water.

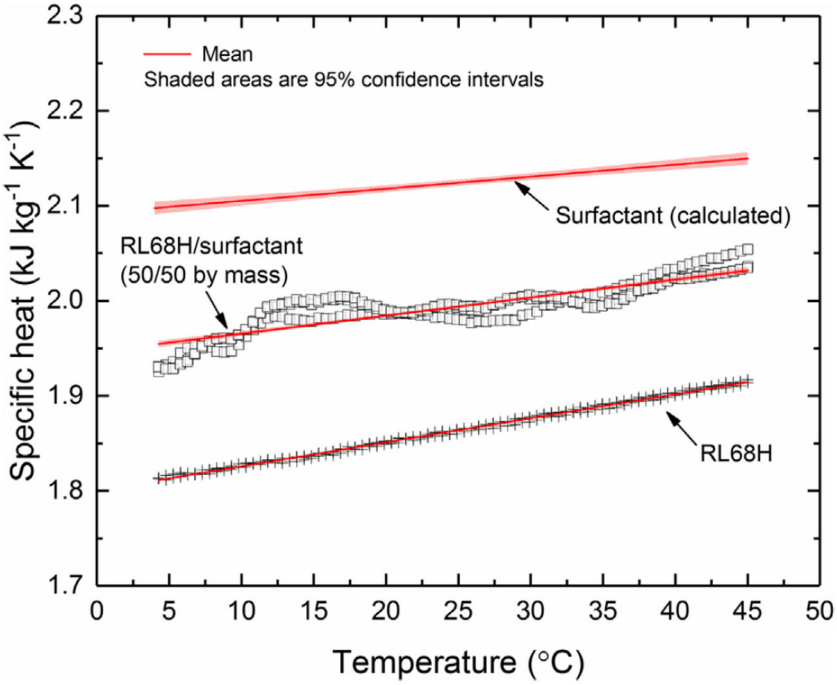

Fig. 4.

Measured specific heats of the neat lubricant (RL68H) and the lubricant/surfactant mixture (50/50 by mass), and the calculated (Eq. (5)) specific heat of the surfactant.

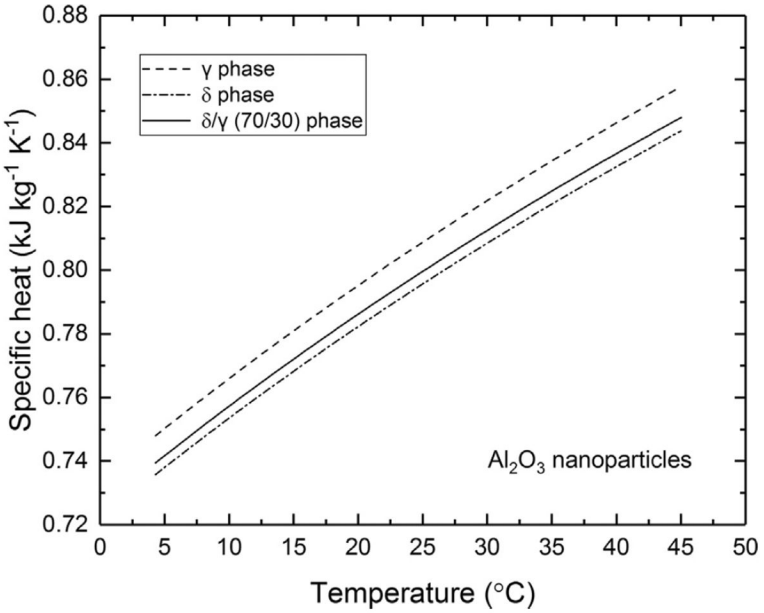

Fig. 5.
Calculated specific heats of the δ-phase, γ-phase, and δ/γ-phase Al_2O_3 nanoparticles.

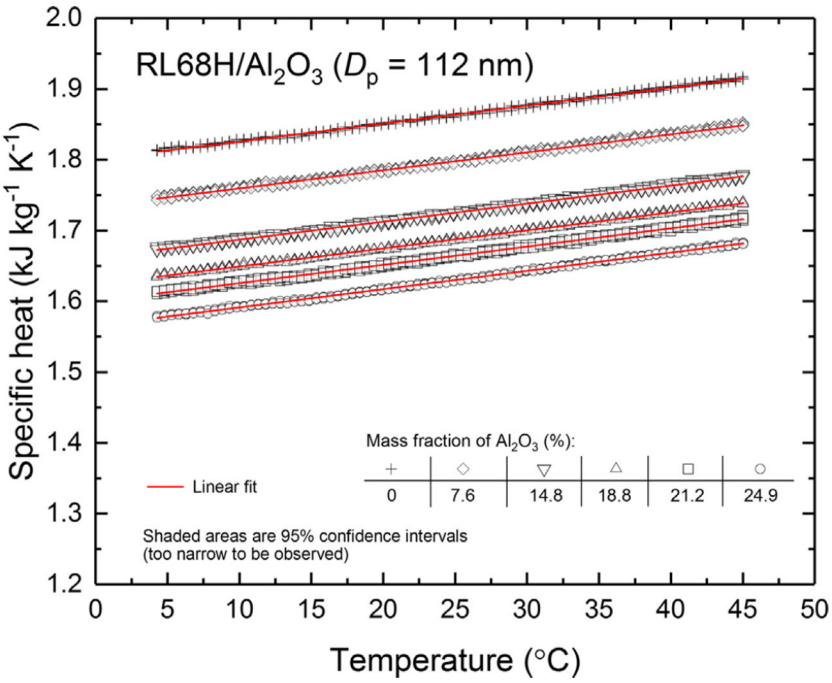

Fig. 6.

Measured specific heats of Al_2O_3 nanolubricants with 112-nm diameter nanoparticles for various mass fractions.

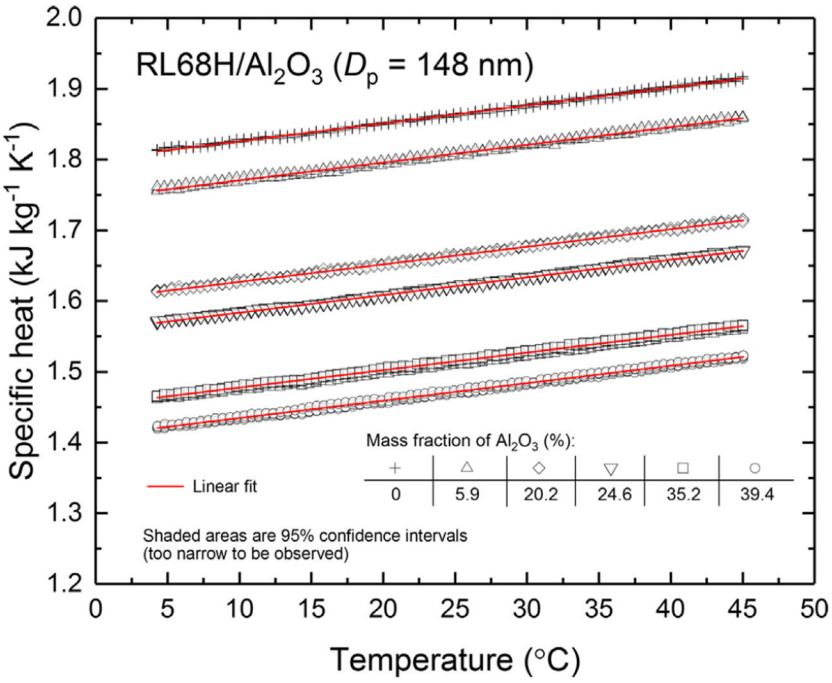

Fig. 7.

Measured specific heats of Al_2O_3 nanolubricants with 148-nm diameter nanoparticles for various mass fractions.

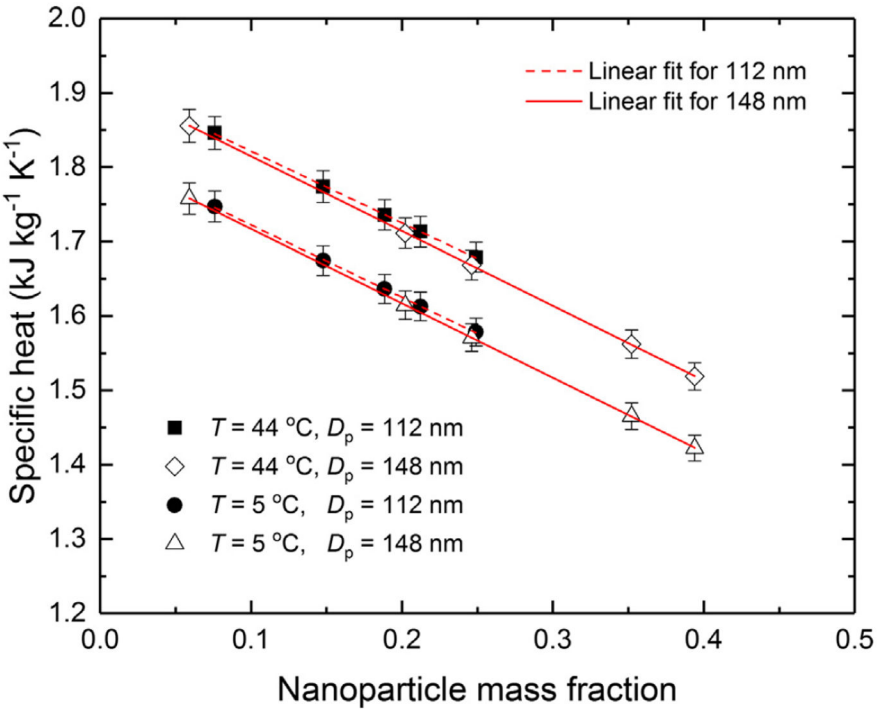

Fig. 8.

Influences of nanoparticle mass fraction, particle size, and temperature on the specific heat of nanolubricant.

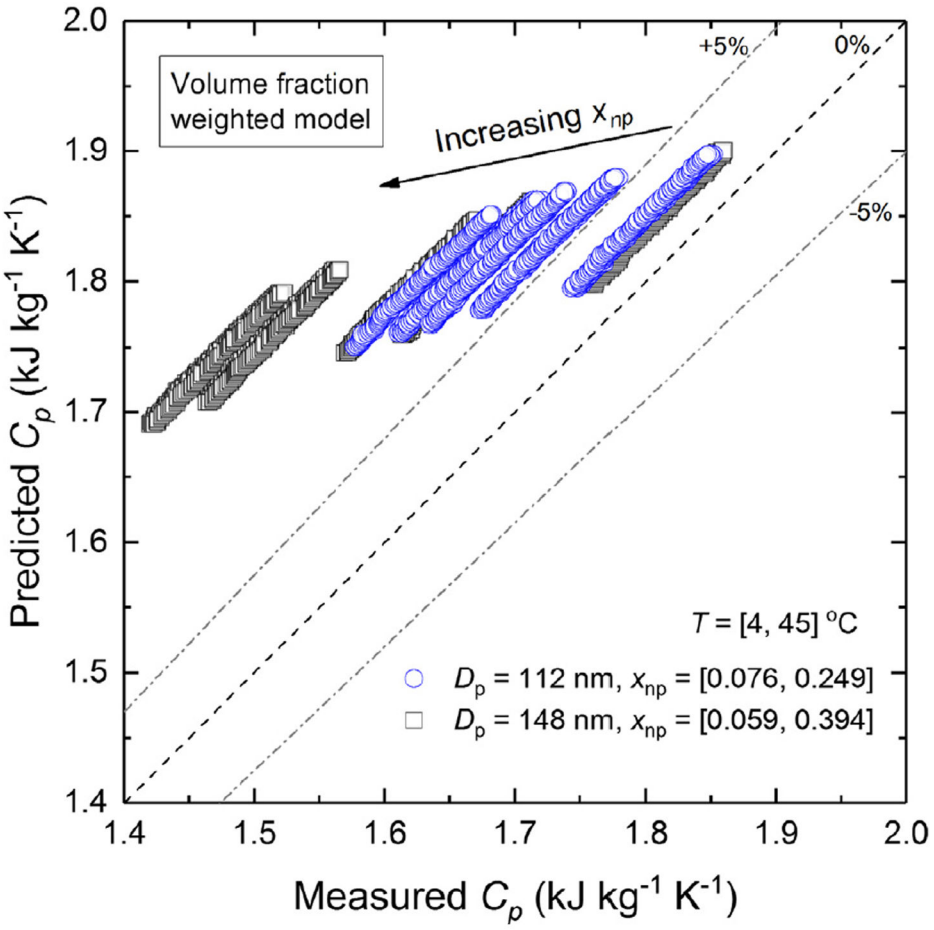

Fig. 9.

Comparison of the measured specific heats of nanolubricants to the predictions calculated by Eq. (7) (the volume fraction weighted model).

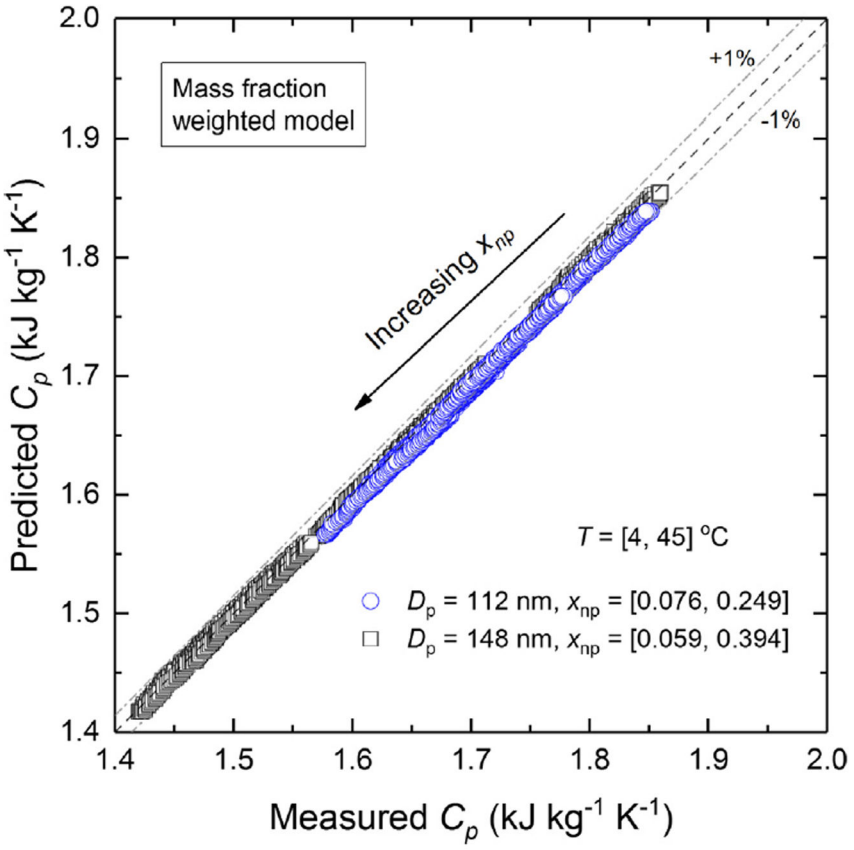

Fig. 10.

Comparison of the measured specific heats of nanolubricants to the predictions calculated by Eq. (8) (the mass fraction weighted model).

Table 1

Diameters, mass fractions, densities, and specific heat fittings for the test fluids.

D_{p0} (nm)	D_p (nm)	x_{np}	x_s	x_L	ρ_m (kg m^{-3})	Linear fit: C_p [kJ kg^{-1} K^{-1}] = A_0 + $A_1 T$[°C]			$U_{r,Cp}$ (%)
						A_0	A_1	Residual standard deviation of fit (%)	
N/A	N/A	0	0	1.0	979.3	1.80043	0.00253	0.11	1.19
N/A	N/A	0	0.5	0.5	N/A	1.94650	0.00190	0.66	1.75
N/A	N/A	0	1	0	938.0	2.09257	0.00127	0.67	1.76
20	112	0.076	0.024	0.900	1034.4	1.73427	0.00254	0.10	1.19
20	112	0.148	0.046	0.806	1095.2	1.66161	0.00255	0.10	1.19
20	112	0.188	0.059	0.753	1132.0	1.62365	0.00255	0.07	1.18
20	112	0.212	0.066	0.721	1154.7	1.59978	0.00258	0.12	1.20
20	112	0.249	0.078	0.673	1191.9	1.56547	0.00258	0.07	1.18
40	148	0.059	0.015	0.926	1023.0	1.74542	0.00251	0.13	1.20
40	148	0.202	0.051	0.747	1145.9	1.60221	0.00248	0.08	1.19
40	148	0.246	0.062	0.692	1190.4	1.55846	0.00250	0.07	1.18
40	148	0.352	0.088	0.560	1312.8	1.45293	0.00248	0.15	1.21
40	148	0.394	0.099	0.508	1368.2	1.40989	0.00247	0.15	1.21

Table 2

Comparison of the nanoparticle mass fractions that were determined by the measured masses to those determined by using the nanolubricant density measurement.

D_{p0} (nm)	D_p (nm)	x_{np} (determined by using nanolubricant density measurement)	x_{np} (determined by measured masses)	Absolute deviation
20	112	0.075	0.076	0.001
20	112	0.148	0.148	0
20	112	0.189	0.188	0.001
20	112	0.213	0.212	0.001
20	112	0.250	0.249	0.001
40	148	0.060	0.059	0.001
40	148	0.203	0.202	0.001
40	148	0.247	0.246	0.001
40	148	0.354	0.352	0.002
40	148	0.396	0.394	0.002

Table 3

Constants for Eq. (6).

Constants	δ-Al_2O_3	γ-$A1_2O_3$
B_1	106.9180	108.6830
B_2	36.62190	37.22630
B_3	−13.97590	−14.20650
B_4	2.157990	2.193601
B_5	−3.157761	−3.209881